Contrib Mineral Petrol (1987) 96:465–475

Contributions to Mineralogy and Petrology

Compositional and thermal convection in magma chambers

Daniel Martin, Ross W. Griffiths, and Ian H. Campbell
Research School of Earth Sciences, Australian National University, Canberra, A.C.T. 2601, Australia

Abstract. Magma chambers cool and crystallize at a rate determined by the heat flux from the chamber. The heat is lost predominantly through the roof, whereas crystallization takes place mainly at the floor. Both processes provide destabilizing buoyancy fluxes which drive highly unsteady, chaotic convection in the magma. Even at the lowest cooling rates the thermal Rayleigh number Ra is found to be extremely large for both mafic and granitic magmas. Since the compositional and thermal buoyancy fluxes are directly related it can be shown that the compositional Rayleigh number Rs (and therefore a total Rayleigh number) is very much greater than Ra. In the case of basaltic melt crystallizing olivine Rs is up to 10^6 times greater than Ra. However compositional and thermal buoyancy fluxes are roughly equal. Therefore thermal and compositional density gradients contribute equally to convection velocities in the interior of the magma. Effects of thermal buoyancy generated by latent heat release at the floor are included.

The latent heat boundary layer at the floor of a basaltic chamber is shown to be of the order of 1 m thick with very low thermal gradients whereas the compositional boundary layer is about 1 cm thick with large compositional gradients. As a consequence, the variation in the degree of supercooling in front of the crystal-liquid interface is dominated by compositional effects. The habit and composition of the growing crystals is also controlled by the nature of the compositional boundary layer. Elongate crystals are predicted to form when the thickness of the compositional boundary layer is small compared with the crystal size (as in laboratory experiments with aqueous solutions). In contrast, equant crystals form when the boundary layer is thicker than the crystals (as in most magma chambers). Instability of the boundary layer in the latter case gives rise to zoning within crystals. Diffusion of compatible trace elements through the boundary layer can also explain an inverse correlation, observed in layered intrusions, between Ni concentration in olivine and the proportion of Ni-bearing phases in the crystallizing assemblage.

Introduction

The importance of thermally induced density differences in the fluid dynamics of magma chambers has been known for some time (e.g., Shaw 1965; Bartlett 1969; Hess 1972), but the recognition that compositionally induced density differences can also have a major influence has been comparatively recent (Turner and Gustafson 1978; Chen and Turner 1980; see also reviews by Huppert and Sparks 1984, and Turner and Campbell 1986). If a magma chamber is wider than it is deep, most of the heat is lost by conduction through the roof (Irvine 1970). This gives rise to an extended source of negative buoyancy at the roof that drives thermal convection. In contrast, crystallization takes place mainly at the floor (Campbell 1978; McBirney and Noyes 1979) and, in the case of a tholeiitic magma crystallizing olivine or bronzite assemblages, or during the crystallization of a calc-alkaline magma, this gives rise to an extended source of positive buoyancy that drives compositional convection. Given that there are two sources of buoyancy contributing to motion in the magma, a description of the convection must include the effects of both thermal and compositional density differences (or buoyancy fluxes), and these are conveniently expressed in terms of two Rayleigh numbers: the thermal Rayleigh number and the compositional Rayleigh number.

This paper presents a series of calculations of both Rayleigh numbers. Since the heat flux controls the rate of crystallization, it controls the compositional convection as well as the thermal convection and the ratio of the compositional Rayleigh number to the thermal Rayleigh number is shown to be fixed for a given magma crystallizing a given set of phases. Only the case of bottom crystallization that releases a flux of light magma is considered. We take, as an example, a mafic magma that crystallizes olivine (as was the case for long periods of time in the Bushveld, Stillwater, Muskox, Great Dyke, Jimberlana and Rhum intrusions, amongst others). Olivine crystallization was chosen because the necessary thermodynamic data are available to model olivine fractionation with confidence. Some preliminary calculations are also presented for orthopyroxene, but the results are less reliable due to the poorer quality of the available data. However, we stress that the conclusions apply equally to any magma chamber in which crystallization depletes the melt in heavy components. The fluid mechanics of convection associated with the release of a dense fluid by crystallization at the floor is still not fully understood and we believe it unwise to attempt to extend the calculations to that system until the physics of the process are better known.

Considering only the case of a light fluid released allows us to ignore problems associated with stacked double-diffu-

Offprint requests to: D. Martin

sive convecting layers since, when a light magma is released by crystallization, liquid layering will not form unless crystallization is taking place on vertical walls or walls sloping inward toward the top. The latter is not the case in most magma chambers, except at the roof. The experiments reported by Huppert et al. (1986) in which layering was observed to develop in aqueous solutions cooled from an outward sloping boundary are unlikely to apply to the very small slope angles commonly observed for magma chamber floors, and there is some question as to whether the rough crystal/liquid interface produced in these experiments is a good model of the magmatic situation (as discussed below). Layering will also be set up when a fresh batch of magma is injected (again see Turner and Campbell 1986) but, as so many of the parameters which characterize the layers remain unpredictable, it is not yet possible to determine the details of the convection within each layer for real magmatic situations. However, layering set up by replenishment will eventually be destroyed by crystallization when a light fluid is released, restoring the homogeneity of the magma chamber.

In the following two sections we show first that purely thermal convection (with no crystallization) will generally be highly turbulent, even for very slowly cooled magma chambers. Next we show that when crystallization is occurring a compositional Rayleigh number is much larger than the thermal Rayleigh number, so that convection is then much more unsteady and disordered than would be the case for purely thermal convection. We go on to determine typical values for parameters which characterize the thermal boundary layer at the roof, and to discuss the nature of the compositional boundary layer and latent heat boundary layer at the floor. Finally some geological consequences of the results are discussed.

Thermal buoyancy effects

Because the heat flux through the boundaries of the fluid is the quantity directly responsible for driving both thermal convection and crystallization, it is appropriate to discuss the problem in terms of a thermal Rayleigh number based on the heat flux. This flux Rayleigh number is defined as:

$$\mathrm{Ra}_f = \frac{g\alpha q h^4}{\nu \kappa_T^2 \rho C_P}, \tag{1}$$

where q is the heat flux through the roof of the magma chamber, and the other terms are defined in Table 1. The flux Rayleigh number is related to the conventional thermal Rayleigh number Ra,

$$\mathrm{Ra} = \frac{g\alpha \Delta T h^3}{\nu \kappa_T}, \tag{2}$$

by

$$\mathrm{Ra}_f = \mathrm{Nu} \cdot \mathrm{Ra}, \tag{3}$$

where the Nusselt number (Nu), is the ratio of actual heat flux to that which would occur in the absence of convection. Thus

$$\mathrm{Nu} = q \cdot \frac{h}{\kappa_T \rho C_P \Delta T}. \tag{4}$$

Table 1. List of symbols used in the text

Symbol	Units	Description
C_p	J kg^{-1} °C^{-1}	Specific heat capacity
C	–	A constant
d_s	m	Width of compositional boundary layer
d_L	m	Width of latent heat boundary layer
d_T	m	Width of thermal boundary layer
D	–	Trace element distribution coefficient
f	kg m^{-2} s^{-1}	Solute flux out of chamber
g	m s^{-2}	Acceleration due to gravity
h	m	Depth of fluid
L	J kg^{-1}	Latent heat of crystallization
K	Wm^{-1} °C^{-1}	Thermal conductivity of magma
q	Wm^{-2}	Heat flux out of chamber
q_L	Wm^{-2}	Flux of latent heat released by crystallization
ΔS	(weight fraction)	Drop in solute content across chamber
t	s	Time
t_L^*	s	Intermittency time-scale for latent heat boundary layer
t_s^*	s	Intermittency time scale for compositional boundary layer
T	°C	Temperature
ΔT	°C	Drop in Temperature across chamber
w	m s^{-1}	Maximum r.m.s. vertical velocity of fluid in chamber
α	°C^{-1}	Thermal expansion coefficient
β	(weight fraction)$^{-1}$	Compositional "expansion" coefficient
κ_s	m^2 s^{-1}	Diffusivity of solute in magma
κ_T	m^2 s^{-1}	Diffusivity of heat in magma
η	poise	Viscosity of magma
ν	m^2 s^{-1}	Kinematic viscosity of magma
ρ	kg m^{-3}	Density of magma at its liquidus
$\left.\frac{\partial T}{\partial s}\right\|_{\mathrm{liq}}$	°C	Slope of liquidus in $T-S$ space
Ra	–	Conventional thermal Rayleigh number
Ra_f	–	Flux-based thermal Rayleigh number
Rs	–	Conventional compositional Rayleigh number
Rs_f	–	Flux-based compositional Rayleigh number
Nu	–	Thermal Nusselt number
Nu_s	–	Compositional Nusselt number

The relationship between the Nusselt number and the Rayleigh number for very large values of the Rayleigh number ($\mathrm{Ra} > 10^5$) is given by (see review by Turner 1973)

$$\mathrm{Nu} = C \cdot \mathrm{Ra}^{\frac{1}{3}}, \tag{5}$$

where C is a numerical constant having an approximate value of 0.10. The precise value of this constant is irrelevant to the conclusions of this paper. Then (3) and (5) give

$$\mathrm{Ra} = \left(\frac{\mathrm{Ra}_f}{C}\right)^{\frac{3}{4}}. \tag{6}$$

The slowest method of cooling a magma chamber is solely by conduction through country rock. It is unclear how much heat is lost through the floor of a magma chamber. However, the geothermal gradient, the fact that the depth of cover above a magma chamber is finite and the insulating effect of crystals accumulating at the floor

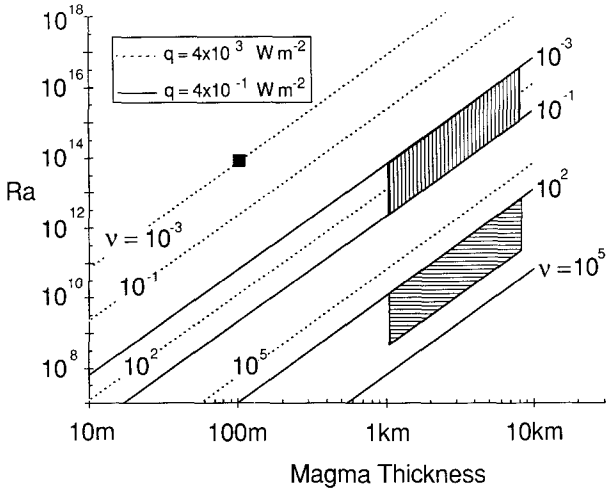

Fig. 1. Ra plotted against h for rapidly cooled chambers (*broken lines*) and slowly cooled chambers (*solid lines*). Lines are plotted for different kinematic viscosities (in $m^2 s^{-1}$) and are labelled accordingly. Fields are plotted for mafic intrusions (e.g., Bushveld, Great Dyke, Stillwater, Jimberlana, *vertically shaded box*) and granitic intrusions (*horizontally shaded box*), both assuming the magmas to be homogeneous over the depth h. The *solid square* shows the approximate position of a 100 m layer of picrite emplaced under a cooler, more fractionated magma

Table 2. Values of parameters used in calculations

Symbol	Units	Value
C_p	$J\,kg^{-1}\,°C^{-1}$	1.1×10^3
C	–	0.10
L	$J\,kg^{-1}$	8.4×10^5
κ_s	$m^2\,s^{-1}$	10^{-10}
κ_T	$m^2\,s^{-1}$	8×10^{-7}

of the chamber, ensure that the heat flux through the roof will be dominant (Irvine 1970; Turner and Campbell 1986). Moreover, we will later argue that the effect of heat less through the floor on convection is unimportant. The minimum estimate of the heat flux from magma chambers several tens of thousands of years old, calculated for cooling by conduction through an infinite roof, is of the order of 0.4 Wm^{-2} while 4 Wm^{-2} is a more reasonable value for steady state heat conduction from a magma chamber buried under a few kilometres of country rock calculated from equations given by Carslaw and Jaeger (1959). Unsteady conductive heat fluxes such as will occur during the first few thousand years after emplacement of a chamber can be orders of magnitude larger than this steady flux. The heat flux will also be higher if cooling is enhanced by any hydrothermal activity, a common feature above magma chambers (e.g., in the Skaergaard; Taylor and Forester 1979).

In other situations heat transfer through the country rock may not be the dominant mechanism for cooling of part of the magma. Such is the case if the magma body is heterogeneous due, for example, to emplacement of a picritic layer underneath a more evolved magma. Here heat transport across the liquid-liquid interface controls crystallization and convection. The heat flux through this double-diffusive interface could be as high as 4×10^3 Wm^{-2} (Huppert and Sparks 1980). We take this as the maximum value for q.

Thermal Rayleigh numbers calculated from equations (1) and (6) for various magma depths and kinematic viscosities are illustrated in Fig. 1. The parameters used in the calculation are listed in Table 2. The simplicity of the approach should be borne in mind: convection is controlled by the heat flux, which in turn is controlled by heat transfer through the overlying country rock or double-diffusive bounding interfaces. Heat fluxes are always larger than 0.4 Wm^{-2}. Hence the inescapable conclusion is that thermal Rayleigh numbers for homogeneous magma chambers are extremely large and therefore purely thermal convection must be highly turbulent. Laminar (cellular) convection is only possible for layer depths of less than 10 m in basaltic chambers and 100 m in granitic chambers, even at the lowest possible cooling rates.

Compositional buoyancy effects

There are two factors which make the floor the major site for crystallization during the early and middle stages of the evolution of a chamber, despite the fact that most of the heat is lost through the roof. First, most basaltic magmas melt the roof of the chamber creating a ponded layer of buoyant contaminated magma with a liquidus temperature appreciably below that of the remainder of the magma in the chamber (Campbell and Turner 1987). The second factor is the well-known pressure effect on the liquidus temperature which causes supersaturation in a homogeneous magma to increase by about 3° C per kilometre of depth in the magma (Jackson 1961). This property implies a larger degree of supersaturation at the bottom of the chamber and consequently more rapid crystallization at the floor than the roof if indeed any crystallization is ocurring at the roof.

The growth of olivine and/or pyroxene crystals at the floor of a mafic magma chamber leaves the fluid next to the crystal/liquid interface depleted in heavy components. The depleted fluid is less dense than the remainder of the magma and convects upward from the growing crystal.

Convection driven purely by compositionally induced buoyancy is analogous to thermal convection and is described in terms of a compositional Rayleigh number Rs, which is defined as

$$\mathrm{Rs}=\frac{g\beta\Delta S h^3}{\nu\kappa_s}, \tag{7}$$

where β is a compositional "expansion" coefficient such that the liquid density, ρ, obeys $\rho=\rho_0(1+\beta\Delta S)$, and ΔS is some (as this stage unknown) concentration difference between top and bottom boundaries. The corresponding flux Rayleigh number is given by

$$\mathrm{Rs}_f=\frac{g\beta f h^4}{\rho\nu\kappa_s^2}, \tag{8}$$

where f is the mass flux out of the liquid due to crystallization of the heavier component – the "solute" S. The quantity $g\beta f$ is the buoyancy flux corresponding to the mass flux f.

The rate of crystallization, and hence the mass flux, is determined by the rate at which the magma cools. The rate of cooling (dT/dt) in turn is determined by two factors:

the rate of heat loss (q) out of the chamber and the rate of release of latent heat of crystallization. Turning the heat conservation equation around we have

$$q=\rho h C_p \frac{dT}{dt}+Lf, \tag{9}$$

where C_p is the specific heat capacity of the magma and L is the latent heat of crystallization. If a constant degree of supersaturation is assumed then the rate of change of magma temperature is also related to the mass flux associated with crystallization through the slope of the liquidus $(\partial T/\partial S|_{liq})$ in the $T-S$ plane:

$$\frac{dT}{dt}=\frac{f}{\rho h}\cdot\left.\frac{\partial T}{\partial s}\right|_{liq}. \tag{10}$$

The factor $1/h$ enters into (10) through the necessity of relating the mass flux onto the crystal pile (in $\mathrm{Kg\,m^{-2}\,s^{-1}}$) to the concentration change in a column of liquid of depth h. The liquidus slope is expressed in °C per weight fraction.

From (9) and (10) the mass flux onto the crystal surface is given by

$$f=\frac{q}{\left(L+C\left.\frac{\partial T}{\partial s}\right|_{liq}\right)}. \tag{11}$$

It now becomes clear why the flux Rayleigh numbers are required: the solute flux is directly related to the heat flux and a priori we know nothing about the appropriate values of concentration differences ΔS (or ΔT) required to evaluate the usual compositional (or thermal) Rayleigh number. The ratio of flux Rayleigh numbers becomes, using (11),

$$\frac{\mathrm{Rs}_f}{\mathrm{Ra}_f}=\left(\frac{\kappa_T}{\kappa_S}\right)^2\frac{C_p\beta f}{\alpha q}$$

$$=\left(\frac{\kappa_T}{\kappa_S}\right)^2\frac{\beta C_p}{\alpha\left[L+C_p\left.\frac{\partial T}{\partial s}\right|_{liq}\right]}. \tag{12}$$

The quantities α, β, $\left.\frac{\partial T}{\partial s}\right|_{liq}$, ν and ρ can be calculated by computer modelling of fractional crystallization for mafic melts crystallizing olivine. The mole fraction of MgO at olivine saturation in mafic melts was obtained from the experiments of Roeder (1975), Arndt (1977) and Campbell and Nolan (unpublished), and the Fe/Mg ratios in the crystallizing olivine from the standard Roeder and Emslie (1970) method. These enable the liquidus temperature to be calculated as a function of wt% olivine removed. Densities were calculated by the method of Bottinga and Weill (1970) using partial molar volume data from Nelson and Carmichael (1979) and Mo et al. (1982). Viscosities were calculated by the method of Shaw (1972).

A similar approach can be used to gain an indication of the effect on convection of orthopyroxene crystallization. In this case it is assumed that the liquidus slope when orthopyroxene is crystallizing is about $\frac{1}{9}$ that when olivine is crystallizing (estimated from the phase diagram for the $MgO-SiO_2$ system given by Bowen and Andersen (1914)).

Typical values calculated for the various parameters are presented in Table 3. Figure 2 is a phase diagram produced by the computer modelling, including superimposed liquid density contours.

Equations (3) and (5) also hold for the compositional Rayleigh number:

$$\mathrm{Nu}_s=C\cdot\mathrm{Rs}^{\frac{1}{3}} \tag{13}$$

and

$$\mathrm{Rs}_f=\mathrm{Nu}_s\cdot\mathrm{Rs}, \tag{14}$$

where Nu_s is the compositional Nusselt number defined by

$$\mathrm{Nu}_s=\frac{hf}{\kappa_s\rho\Delta S}, \tag{15}$$

where ΔS is in weight fraction. The corresponding compositional version of (6) gives $\mathrm{Rs}\sim\left(\frac{\mathrm{Rs}_f}{C}\right)^{\frac{3}{4}}$ where the constant

Table 3. Calculated parameters for various fluids

	Bushveld U[a] magma	Great Dyke[b] parent	MORB[c] picrite	Great Dyke[d] evolved	$Na_2CO_3\cdot10H_2O$[e] aq. solution
Phase on liquidus	ol.	ol.	ol.	opx.	$Na_2CO_3\cdot10H_2O$
α (°C^{-1})	5.46×10^{-5}	6.45×10^{-5}	7.91×10^{-5}	6.40×10^{-5}	4.26×10^{-4}
β	9.16×10^{-2}	7.30×10^{-2}	4.26×10^{-2}	2.90×10^{-2}	8.59×10^{-1}
$\left.\frac{\partial T}{\partial s}\right\|_{liq}$ (°C)	7.01×10^{2}	7.14×10^{2}	6.89×10^{2}	0.795×10^{2}	0.507×10^{2}
ν (m^2 s^{-1})	4.63×10^{-2}	1.66×10^{-2}	3.77×10^{-3}	7.65×10^{-1}	1.79×10^{-5}
η (poise)	1.21×10^{2}	4.38×10^{1}	1.01×10^{1}	1.99×10^{3}	1.89×10^{-2}
ρ (kg m^{-3})	2.613×10^{3}	2.643×10^{3}	2.712×10^{3}	2.616×10^{3}	1.107×10^{3}
$\mathrm{Rs}_f/\mathrm{Ra}_f$	7.33×10^{7}	4.29×10^{7}	2.13×10^{7}	2.90×10^{7}	1.87×10^{6}
Rs/Ra	7.92×10^{5}	5.30×10^{5}	3.14×10^{5}	3.95×10^{5}	5.06×10^{4}

[a] Irvine et al. (1983)
[b] Wilson (1982)
[c] Elthon (1979)
[d] Composition 2 after fractional crystallization of 23 wt% olivine
[e] 30 wt% solution, parameters derived from International Critical Tables

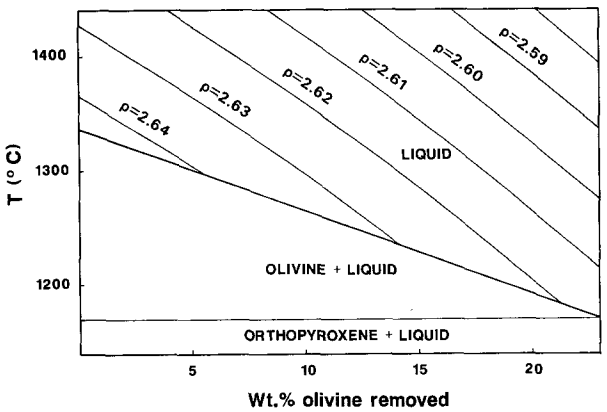

Fig. 2. Calculated phase diagram for the parental liquid of the Great Dyke (Wilson 1982) undergoing olivine fractionation, contoured for density (in g cm^{-3})

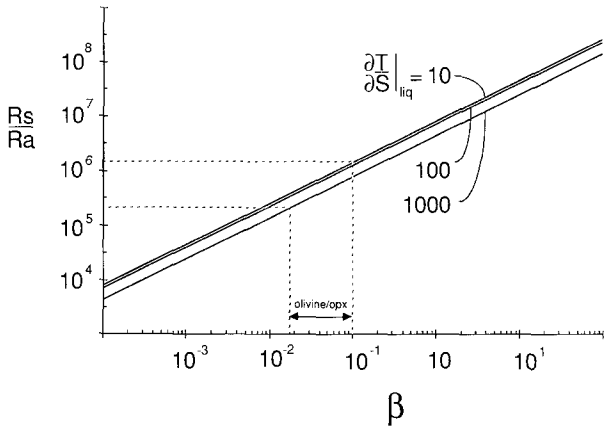

Fig. 3. The ratio of conventional Rayleigh numbers Rs/Ra against β (in 'per weight fraction') for various values of $\left.\frac{\partial T}{\partial s}\right|_{liq}$ (°C per weight fraction) using $\rho = 2500$ Kg m^{-3} and $L = 8.4 \times 10^5$ J Kg^{-1} although, as discussed in the text, this graph is believed to have general applicability

$C \approx 0.1$ (as for thermal convection) and the ratio of the conventional Rayleigh numbers is given by

$$\frac{\mathrm{Rs}}{\mathrm{Ra}} = \left(\frac{\mathrm{Rs}_f}{\mathrm{Ra}_f}\right)^{\frac{3}{4}}. \tag{16}$$

Typical values for Rs/Ra while olivine or pyroxene is crystallizing as shown in Table 3 are of the order of 10^6 while the ratio of flux Rayleigh numbers is of the order of 10^7. Figure 3 shows how the ratio varies as a function of the density coefficient β for various values of the liquidus slope. Variations of the liquidus slope have only a small effect. The value for the latent heat L used in the construction of this diagram was that appropriate to olivine but inspection of equation (12) reveals that the error introduced by this approximation is likely to be much less than an order of magnitude. As minerals crystallizing after olivine have lower latent heats of crystallization, the values for Rs/Ra shown in Fig. 3 are minimum estimates.

An effective Rayleigh number Ra_e, when both compositional and thermal buoyancy forces are destabilizing may be defined by (Turner 1973, p. 255)

$$\mathrm{Ra}_e \equiv \mathrm{Ra} + \mathrm{Rs}. \tag{17}$$

Since Rs is orders of magnitude greater than Ra, $\mathrm{Ra}_e \approx \mathrm{Rs}$.

Taking values of Ra from Fig. 1 and the ratio of Rs/Ra from Fig. 3, we find that the compositional Rayleigh number for mafic magmas crystallizing olivine-orthopyroxene assemblages lies between 10^{18} and 10^{22} for layer depths between 1 and 10 km. At these Rayleigh numbers convection is highly unsteady and disordered (commonly described as turbulent). Laminar, cellular convection is only possible if the heat flux is low and the layer depth is less than 10 cm. Compositional convection decreases as β decreases, but it is interesting to note that β would have to fall below 10^{-8} for the thermal Rayleigh number to be as large as the compositional Rayleigh number.

Bottom crystallization also releases latent heat, providing a second source of thermal buoyancy. However, since the rate of crystallization is controlled by heat loss through the roof, the latent heat flux q_L must be less than the heat flux q through the roof (about one half in the case of olivine crystallization). Thus the buoyancy flux due to latent heat release at the floor is smaller than the thermal buoyancy flux due to cooling through the roof and has a negligible effect on the magnitude of the effective Rayleigh number.

The velocity w of convective motions on the scale of the fluid depth is determined by the sum of buoyancy fluxes due to crystallization, roof cooling and latent heat release. This velocity is given by

$$w \approx \left[\frac{gh}{2\rho}\left(\frac{\alpha q}{C_P} + \beta f + \frac{\alpha q_L}{C_P}\right)\right]^{\frac{1}{3}}, \tag{18}$$

where the factor of two appears in the denominator because each of the fluxes in the summation passes through only one of the boundaries. For mafic magmas crystallizing olivine the thermal buoyancy flux ($g\alpha q/C_P$) due to cooling at the roof is approximately equal to the compositional buoyancy flux ($g\beta f$). The latent heat buoyancy flux is about one half the other two fluxes. This means that, despite the large disparity in Rayleigh numbers, the velocity of convection depends on thermal and compositional effects to roughly equal extents. The maximum velocity is only about 35% larger than it would be if no crystallization were occurring.

Boundary layers

A detailed description of the fluid dynamics of convecting magmas involves the concept of a boundary layer. As buoyancy is produced at the roof or the floor a density inversion builds up in a boundary layer. The buoyant boundary layers grow by diffusion, their thickness increasing with time according to $d = \sqrt{(\pi \kappa t)}$, until at a critical time, t^*, the local Rayleigh number *based on the boundary layer thickness* reaches its critical value, $\mathrm{Ra} \sim 10^3$. At this time the boundary layer becomes unstable (Turner 1973) and the buoyant fluid breaks away to join convection in the interior of the magma.

In the case of magma chambers there are three boundary layers that need to be considered: the thermal boundary layer at the roof, the compositional boundary layer at the floor and a thermal boundary layer produced by latent heat released at the floor.

The upper thermal boundary layer

The heat flux q through the roof must all pass through the upper thermal boundary layer. We approximate the in-

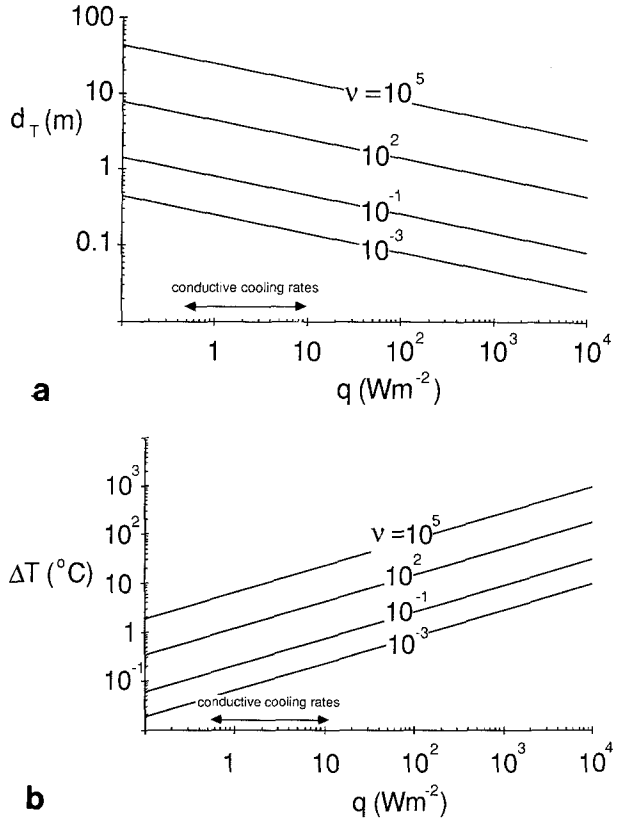

Fig. 4. a The thickness of the thermal boundary layer and **b** the temperature difference across the thermal boundary layer as functions of cooling rate for different viscosities. The likely normal range of conductive cooling rates is indicated

termittently unstable boundary layer described above by a boundary layer of constant thickness across which heat is transported solely by steady state conduction, so that

$$d_T = \kappa_T \rho C_P \frac{\Delta T}{q}. \tag{19}$$

Since convective stirring keeps the magma homogeneous outside the boundary layers, the temperature drop across the thermal boundary layer in (19) is equal to the overall temperature difference ΔT available to drive convection. Combining equation (19) with (1, 4, 5 and 6) it follows that the boundary layer thickness scales as the inverse of the Nusselt number:

$$d_T = \frac{h}{\mathrm{Nu}} = \left[\frac{\rho C_P \nu \kappa_T^2}{C^3 g \alpha q}\right]^{\frac{1}{3}} \tag{20}$$

and

$$\Delta T = \frac{q h}{\kappa_T \rho C_P \mathrm{Nu}} = (\nu/g\alpha\kappa_T^2)^{\frac{1}{3}} (q/\rho C_P C)^{\frac{2}{3}}. \tag{21}$$

Figure 4 illustrates the values of the thermal boundary layer thickness and ΔT given by equations (20) and (21) as functions of heat flux and magma viscosity. The upper thermal boundary layer thickness is generally between 10 cm and 1 m for mafic magmas or 5 m and 50 m for granitic magmas. The corresponding temperature difference lies between 0.05 and 1° C for mafic magmas and between 1 and 50° C for granitic magmas. These quantities can be evaluated more precisely for specific cases.

The compositional and latent heat boundary layers

Latent heat is generated at the crystal/liquid interface as crystallization proceeds so that not only is compositional buoyancy produced at the lower boundary, but thermal buoyancy as well. There are thus two superimposed boundary layers at the base of the magma chamber: the compositional boundary layer and the latent heat boundary layer.

The latent heat flux is related to the heat flux through the roof by the following equation:

$$q_L = fL = \frac{qL}{\left(L + C_P \left.\frac{\partial T}{\partial s}\right|_{\mathrm{liq}}\right)}, \tag{22}$$

and q_L is generally of order $q/2$ when olivine is crystallizing from a mafic magma.

If the timescale t_L^* for the conductive growth and sweeping away of the latent heat boundary layer alone is shorter than the corresponding timescale t_S^* for the compositional boundary layer alone, then the compositional boundary layer will never reach its maximum thickness calculated in the absence of the latent heat boundary layer: instability of the latent heat boundary layer on the shorter timescale will sweep away the buoyant (but always stable) compositional boundary layer. Conversely, if the intermittent timescale for the chemical boundary layer is smaller than t_L^*, the latent heat boundary layer will not reach its full thickness due to instability of the chemical boundary layer. We can say that the smaller of the two timescales calculated for the independent boundary layers is the timescale applicable to the double boundary layer. This is because of the large disparity in length scales (d_L, like d_T, is of order one hundred times larger than d_s), which means that the buoyancy contained in one boundary layer has little effect on the stability of the other. For independent (uncoupled) boundary layers the timescale t^* can be calculated using the definition of the flux Rayleigh number but substituting $d_s = \sqrt{(\pi \kappa_S t^*)}$ or $d_T = \sqrt{(\pi \kappa_T t^*)}$ as the length-scale in place of the layer depth h. The ratio of the critical timescales for the two lower boundary layers, assuming no coupling, is found from (1), (8) and (22):

$$\frac{t_S^*}{t_L^*} = \left[\frac{\alpha q_L}{C_P \beta f}\right]^{\frac{1}{2}} = \left(\frac{\alpha L}{\beta C_P}\right)^{\frac{1}{2}}. \tag{23}$$

For magmas crystallizing olivine we find $t_S^*/t_L^* \approx 0.8$. Hence the timescales for the latent heat boundary layer and the compositional boundary layer are almost identical, and parameters governing each boundary layer can be determined as if the other boundary layer were not present.

Having established the effective independence of the superimposed boundary layers we can now calculate d_s and ΔS in a manner directly analogous to the calculation of d_T and ΔT in (20, 21) above. Thus from (2) and (12) we find

$$d_s = \frac{h}{\mathrm{Nu}_s} = \frac{d_T \mathrm{Nu}}{\mathrm{Nu}_s} = d_T \left(\frac{\mathrm{Ra}_f}{\mathrm{Rs}_f}\right)^{\frac{1}{3}} = \left[\frac{\rho \nu \kappa_s^2}{C^3 g \beta q}\left(L + C_P \left.\frac{\partial T}{\partial s}\right|_{\mathrm{liq}}\right)\right]^{\frac{1}{3}}, \tag{24}$$

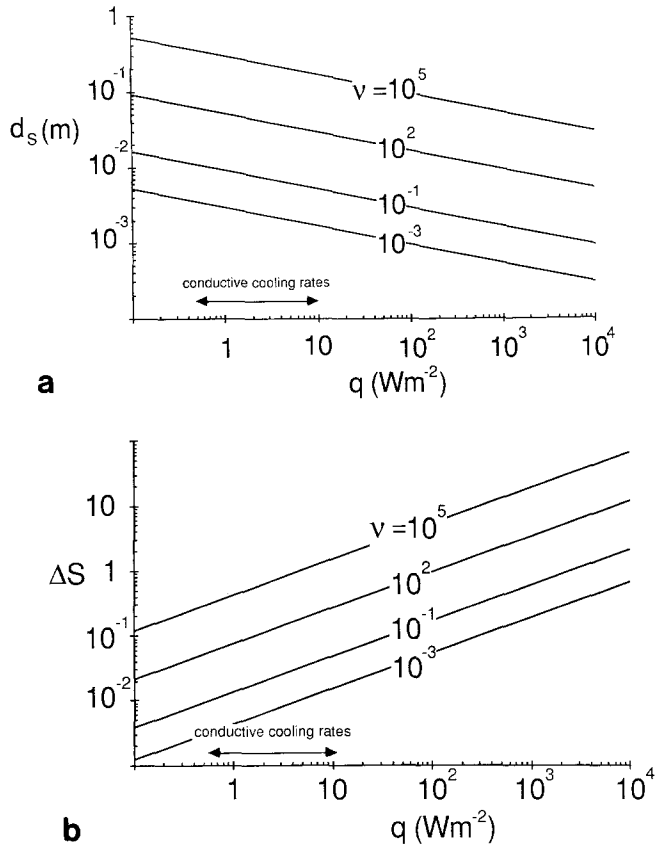

Fig. 5. a The thickness of the compositional boundary layer and **b** the compositional difference ΔS across the compositional boundary layer as a function of cooling rate for different viscosities for magmas crystallizing olivine. Note that ΔS is expressed as a weight fraction, to convert into weight percent multiply by 100. Again the likely normal range of conductive cooling rates is indicated

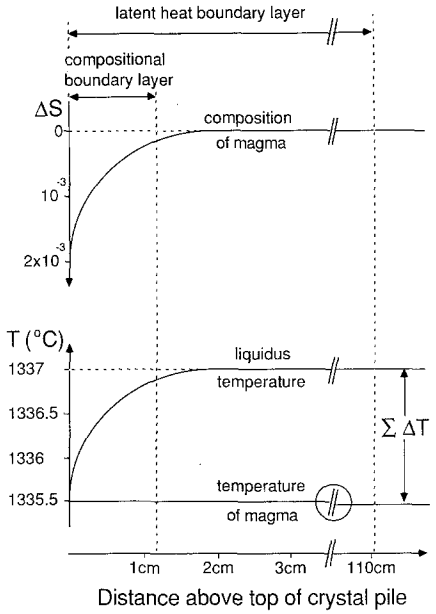

Fig. 6. A sketch of chemical and thermal profiles in the compositional and latent heat boundary layers at the base of a magma chamber. The numbers shown are those calculated for the parental magma of the Great Dyke (Wilson 1982) cooling at 4×10^{-1} Wm^{-2} in a 3 km deep chamber, but the qualitative form of the diagram is appropriate to all magmas which release a light fluid on crystallization. Note that the depletion of the magma in the crystallizing components across the compositional boundary layer leads to a sharp decrease in the liquidus temperature close to the growing crystals. Also note that the total amount of supercooling ($\Sigma\Delta T$) always increases away from the crystal/liquid interface, and that compositional effects contribute by far the largest portion of this supercooling. The slope of the line representing magma temperature is reflected in the (small) drop across the break between 3 cm and 110 cm (*circled in the diagram*)

while from (24) and (11) we obtain

$$\Delta S=\frac{f d_s}{\rho\kappa_s}=\left(\frac{\nu}{g\beta\kappa_s^2}\right)^{\frac{1}{4}}\left[\frac{q}{\rho C\left(L+C_P\left.\frac{\partial T}{\partial s}\right|_{\text{liq}}\right)}\right]^{\frac{3}{4}}. \tag{25}$$

Figure 5 illustrates the values found for d_s and ΔS when olivine is crystallizing from a mafic magma chamber. The compositional boundary layer is roughly one hundred times thinner than the (upper) thermal boundary layer, with d_s $\sim$2 mm to 2 cm. Corresponding values of ΔS are 0.2 to 4 wt.%. It is interesting to note that the density deficit $\beta\Delta S$ is two orders of magnitude greater than the density difference $\alpha\Delta T$, since

$$\beta\Delta S/\alpha\Delta T=(\kappa_T/\kappa_S)^{\frac{1}{4}}\left[\beta C_P/\alpha\left(L+C_P\left.\frac{\partial T}{\partial s}\right|_{\text{liq}}\right)\right]^{\frac{3}{4}}\approx(\kappa_T/\kappa_S)^{\frac{1}{4}}.$$

Together with the disparate boundary layer thicknesses this implies that the compositional boundary layer and the (upper) thermal boundary layer contain roughly equal amounts of buoyancy.

The form of the lower boundary layer becomes clearer if we consider a specific example. The example we have chosen is a magma of Great Dyke composition crystallizing olivine. The results are illustrated in Fig. 6. It has been assumed that the total thickness of the magma is 3 km and that $q=0.4$ Wm^{-2}; the temperature of crystallization is calculated to be 1337° C. The following points are noteworthy.

(i) The temperature increases towards the top of the crystal pile (here considered to be a planar surface) because crystallization at the floor results in the release of a significant amount of latent heat.

(ii) The thickness of the latent heat boundary layer is 110 cm compared with 1.1 cm for the compositional boundary layer.

(iii) The calculated temperature drop across the latent heat boundary layer is 0.02° C, resulting in a *very* small thermal gradient.

(iv) The change in the olivine content of the melt across the compositional boundary layer is 0.2 wt%, resulting in a strong compositional gradient close to the growing crystals.

(v) The depletion of the olivine component of the melt within the compositional boundary layer lowers the liquidus temperature of the magma adjacent to the growing crystal by 1.5° C compared with the liquidus temperature of the far field magma.

(vi) If the melt adjacent to the crystals at the top of the crystal pile is assumed to be in equilibrium with the crystals, the far field magma is supercooled by 1.5° C, almost all of which (1.48° C) is due to compositional depletion in the boundary layer and only 0.02° C is due to thermal differences. That is, the supercooling of the magma outside the

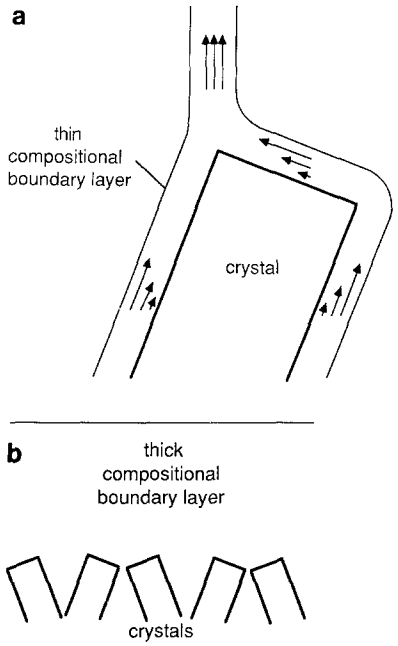

Fig. 7. Sketches of the two possible configurations of compositional boundary layer and growing crystals. **a** At high cooling rates for the least viscous magmas the crystals are large compared with the thickness of the boundary layer. The size of the *arrows* is intended to indicate the speed of fluid moving in the boundary layer. **b** In most situations the crystals are small compared with the thickness of the boundary layer, which in this case grows by diffusion and breaks down periodically

boundary layers (i.e., the bulk of the magma) is dominated by compositional effects and is more appropriately described as supersaturation (or, equivalently, as constitutional supercooling).

(vii) Supersaturation (supercooling) increases with distance from the crystal-liquid interface.

Discussion

The influence of compositional boundary layer thickness on crystal habit

Our calculations show that for crystals growing at the bottom of a convecting silicate melt, the length-scale for the compositional boundary layer (Fig. 5a) will normally be greater than that of the crystals (observed to be ≤ 3 mm), although thin boundary layers are possible under some conditions. Similar calculations show that when crystals are grown from aqueous solutions in laboratory tanks the thickness of the compositional boundary layers will always be less than the size of the crystals. The latter crystals, if growing at the bottom of a convection tank, are large and elongated regardless of whether cooling is from the bottom or top of the tank, whereas crystals in cumulate rocks are more equant. We believe that this fundamental difference in crystal habit is due to the difference in the relative thickness of the boundary layer from which the crystals grew, and can therefore be predicted from a knowledge of the convection regime and crystal size.

An example of a relatively thin compositional boundary layer is illustrated in Fig. 7. Thin compositional boundary layers "cling" to the sides of the growing crystal and are inhibited from breaking away by viscous stresses. There is no motion of fluid at the crystal surface but velocities within the boundary layer increase with distance from the crystal, reaching a maximum at the outer edge of the buoyant layer. Since the fluid released is light it flows upwards as illustrated in Fig. 7a and eventually leaves the crystal from its highest point as a plume. Removal of the depleted fluid from the growing crystal is a continuous process and the system quickly evolves to a steady state. The compositional profiles within the boundary layer are controlled by a balance between diffusion and advection of the buoyant layer, with the melt adjacent to the growing crystal being strongly depleted in those components which are required to form the solid. The heterogeneous nucleation of new crystals within the boundary layer requires the supercooling adjacent to the crystal to exceed some finite value (note that this value is appreciably less than the value required for homogeneous nucleation outside the boundary layer). If crystal growth and the steady state condition of the boundary layer maintains the degree of supercooling of the fluid at a level below that required for the nucleation of new crystals the existing crystals continue to grow outward, resulting in the formation of elongate crystals.

The relationship between the compositional boundary layer and the growing crystals when the boundary layer thickness is greater than the size of the crystals is very different. This configuration is illustrated in Fig. 7b. Under these conditions there is no continuous, steady flow of buoyant fluid away from the growing crystals. Molecular diffusion spreads the chemical depletion through a much greater distance before the boundary layer acquires enough buoyancy to become unstable and to rise as a plume. As a consequence the boundary layer thickness is continuously changing and is intermittently thinned each time it is "swept" by a plume. It then thickens slowly by diffusion as crystallization proceeds. The composition of the fluid adjacent to the growing crystal must change constantly in response to the irregular fluctuations in the thickness of the boundary layer. When the boundary layer is thin the composition of the magma adjacent to the crystal is closer to that of the undepleted, far field magma outside the boundary layer. When the boundary layer is at its maximum width, near the end of the diffusive growth, the magma is most depleted and close to the equilibrium composition. This means that the degree of supercooling of the magma adjacent to the crystal is constantly changing, being highest early in the growth cycle and lowest immediately before the end of the cycle. These fluctuations allow the supercooling at the crystal-liquid interface to occasionally exceed that required for the nucleation of new crystals, even though the average supercooling may be less than that in the narrow-boundary layer case. The result is that new crystals can nucleate against existing crystals, leading to a more equant crystal habit.

The influence of the compositional boundary layer on trace element partitioning

Transport of material to the growing crystal is ultimately by diffusion across the compositional boundary layer. Trace elements which partition preferentially into the growing crystal will become depleted within the boundary layer by an amount which is dependent on both the diffusion coefficient (κ_{tr}) and the partition coefficient (D) for the element. We approximate this process by assuming steady-state dif-

fusion across the time-averaged thickness ($2/3\,d_s$) of the compositional layer. Then the apparent distribution coefficient D', which we define as the ratio of the element concentration in the crystal to that in the far field magma outside the boundary layer, is given by

$$D' = \frac{D}{1 + \frac{2Dfd_s}{3\rho\kappa_{tr}}}, \tag{26}$$

where, from (24) and (11),

$$\frac{Dfd_s}{\rho\kappa_{tr}} = D\left[\frac{\kappa_s^2 q^3 \nu}{C^3\rho^3 g\beta\kappa_{tr}^4\left[L + C_P\left.\frac{\partial T}{\partial S}\right|_{liq}\right]^3}\right]^{\frac{1}{4}}. \tag{27}$$

Thus D' will be appreciably less than D when $\frac{Dfd_s}{\rho\kappa_{tr}}$ is of order one or greater. For example, for Ni in olivine crystallizing from a basaltic melt $\kappa_{tr} \sim \kappa_s$ and $D \sim 10$. Putting appropriate values into equation (26) reveals that D' is significantly less than D for cooling rates of 40 Wm^{-2} or greater. For trace elements with small diffusivities (i.e., ions with large charges and small radii) the effect is even greater. The appropriate partition coefficient of crystallization from silicate melts is therefore not the equilibrium partition coefficient D but the apparent coefficient D' which depends not only on the composition of the melt and temperature of crystallization but also on the nature of the convection. We suggest that the use of equilibrium partition coefficients in geochemical modelling can lead to significant errors, especially in the case of highly compatible trace elements.

Detailed studies of the chemistry of minerals in rhythmically layered sequences from the Skaergaard intrusion by McBirney and Noyes (1979) support our arguments concerning the nature of the boundary layer. McBirney and Noyes have shown that the concentration of elements with high partition coefficients into a mineral or group of minerals depend on the abundance of that mineral or group of minerals in the rock. For example, the concentration of Ni in olivine is lowest at the bottom of a rhythmic layer and increases towards the top. The bottoms of the rhythmic layers are rich in olivine, pyroxene and oxides and grade into a top which is plagioclase-rich. (Note that since iron-oxide, olivine and pyroxene are major phases in the crystallizing assemblage the magma released by crystallization in this instance is light.) The partition coefficient for Ni into olivine, pyroxene and the oxides is greater than one but for plagioclase it is very low. Thus there is an inverse correlation between the Ni content of olivine in a rock and the abundance of Ni-rich phases in that rock. This observation requires the Ni content of the melt from which the olivines are growing to vary systematically with the amount of Ni-rich phases crystallizing. Because the amount of Ni-rich phases in an individual layer is small compared with the size of the main body of magma, the Ni concentration of the far field magma cannot change significantly during the crystallization of a single layer. The crystallization of Ni-rich phases in an individual rhythmic layer could, however, influence the Ni content of a narrow boundary layer.

There are two cases to consider: the first when the length scale for the boundary is less than that of the crystal and the second when it is greater.

If the boundary layer is thin it is influenced only by the adjacent crystal. The boundary layer on each olivine crystal at the top of the crystal pile will be depleted in Ni so that the Ni content of the crystallizing olivines will be less than the equilibrium value. Because the length scale of the boundary layer is small compared with that of the crystal, boundary layers will rarely overlap. Hence the Ni content of the boundary layer on a given olivine crystal will not normally be influenced by the crystallization of other Ni-rich phases within the layer. If boundary layers are thin there should therefore be no correlation between the Ni content of olivine in a rock and the abundance of Ni-rich phases in that rock.

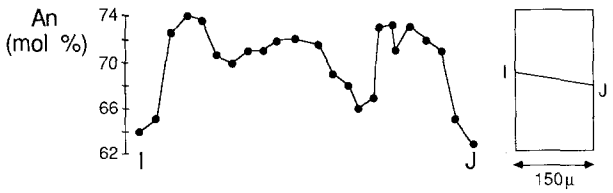

Fig. 8. Compositional variations determined by electron microprobe along a traverse IJ across a zoned placioclase crystal from the Jimberlana intrusion

If the compositional boundary layer is thicker than the crystals, the boundary layer is not specific to an individual crystal but forms a continuum (as shown in Fig. 7b). Growth of each crystal influences the Ni content of the boundary layer, so that the higher the percentage of Ni-rich phases crystallizing (and the higher their partition coefficient), the lower the Ni content of the boundary layer fluid. Thus the observed inverse correlation between the Ni content of olivines and the abundance of Ni-rich phases in the Skaergaard intrusion is consistent with the length scale of the boundary layer being greater than that of the crystal. Similar observations have been made for the Jimberlana intrusion (Campbell 1978).

Zoning in crystals

As pointed out earlier, if the compositional boundary layer is thick compared with the crystals the composition of the melt adjacent to the crystal/liquid interface is continually changing on a cyclic basis. Cycles are not periodic in this highly unsteady, chaotic flow, but have a time scale $t_s^* \sim d_s^2/\pi\kappa_s$. Taking $d_s \sim 1$ cm and $\kappa_s = 10^{-10}$ $m^2\,s^{-1}$ gives $t_s^* \sim 3$ to 4 days. By way of comparison the rate of advance of the crystal pile is of the order 10 cm $year^{-1}$, making the time scale for the growth of a 2 mm crystal about 7 days. The similarity of the two time scales suggests that crystals growing in magma chambers should show compositional banding.

Our model can be tested by looking for oscillatory zoning in crystals from layered intrusions. Unfortunately diffusion is rapid in most crystals and any zoning which forms during primary crystallization is annealed during the slow cooling of a large intrusion. Diffusion rates in plagioclase however are very much slower and plagioclase crystals do preserve their primary zoning. Campbell (1973) made a detailed study of zoning in cumulus plagioclase crystals of gabbros from the Jimberlana Intrusion. He found that cores of plagioclase crystals from both pyroxene and plagioclase-rich layers showed complex oscillatory zoning. An example from a mesocumulate pyroxene-rich layer is illustrated in Fig. 8. Note that the predicted oscillations are present and

of a magnitude comparable to the ΔS predicted (albeit for olivine) in Fig. 5b.

Crystallization in the thermal boundary layer

Brandeis and Jaupart (1986) and Morse (1986), following Wager and Deer (1939), have developed models for crystallizing magmas in which crystals nucleate and grow in the (upper) thermal boundary layer. This requires the temperature drop across the boundary layer to be large enough to enable homogeneous nucleation to occur there in preference to heterogeneous nucleation against the walls and floor of the chamber.

We have shown (Fig. 4b) that the temperature drop across the thermal boundary layer in mafic magma chambers is usually of the order of 0.05° C to 1° C, and is always less than 10° C, except at extremely high cooling rates. Thus the predicted temperature drops are usually far too low to enable homogeneous nucleation to occur in the thermal boundary layers of basaltic magma chambers. For viscous granitic chambers ΔT is predicted to be between 1° C and 10° C for slow to moderate cooling rates, and considerably larger at higher cooling rates but this is at least partially offset by the increased difficulty of nucleation in granitic magmas. We consider it unlikely that the thermal boundary layer is an important site for homogeneous nucleation in most granitic chambers.

The effect of heat loss from the floor

Experimental and theoretical studies of the effect of cooling a magma chamber from the floor as well as the roof are reported in Jaupart et al. (1984) and Jaupart and Brandeis (1986). Unfortunately these studies were carried out using a non-crystallizing fluid. Cooling from the bottom in this case merely results in the diffusion-controlled growth of a cold, dense stagnant layer. The situation when crystallization is taken into account is completely different. Superimposed on the stabilizing (negative) buoyancy flux resulting from cooling are two fluxes of destabilizing (positive) buoyancy: the light depleted fluid released by crystallization and the hot light fluid resulting from the concomitant release of latent heat. Note that both of these destabilizing buoyancy fluxes would be *enhanced* by any additional heat loss from the floor. The stabilizing effect of cooling through the floor is completely overwhelmed by the destabilizing effects of crystallization (i.e., $(\beta f/\kappa_S^2) \gg (\alpha q'/\kappa_T^2)$, where q' is the heat flux through the floor less the latent heat flux). This would be true even if the heat flux through the floor were comparable to the heat flux through the roof. In magma chambers where crystallization is occurring under normal conditions at the floor releasing a light depleted fluid there can be absolutely no possibility of a lower stagnant layer forming.

Conclusion

We have evaluated the fundamental parameters controlling convection in a homogeneous magma chamber which is cooled from the top and releases a light fluid on crystallization at the floor. We conclude that magma chambers commonly undergo extremely vigorous convection. The compositional Rayleigh number is much greater than the thermal Rayleigh number: compositional effects control the unsteadiness of the convective motion, especially near the growing crystals. However, the contributions to the total buoyancy flux of cooling and crystallization are comparable and equally important in determining the velocity of convection.

Convection involves three fluid dynamical boundary layers: the thermal boundary layer at the roof and the compositional and latent heat boundary layers at the floor. The nature of the compositional boundary layer in particular has important consequences for the shape and composition of the growing crystals. We suggest that the morphology of the crystals is determined by the relative thickness of the compositional boundary layer compared with the size of the crystals. Zoning is explained as the product of the intermittent instability of the boundary layer whereas the necessity for crystallizing components to diffuse across this boundary layer limits the partitioning of compatible trace elements at moderate to fast cooling rates.

Acknowledgements. The authors are grateful to Stewart Turner and a reviewer for constructive comments and to Karen Buckley and Ross Wylde-Browne for assistance with the preparation of the manuscript. DM acknowledges receipt of an ANU Ph.D. scholarship.

References

Arndt NT (1977) The partitioning of nickel between olivine and ultrabasic and basic komatiitic liquids. Carnegie Inst Washington Yearb 76:553–556

Bartlett RW (1969) Magma convection, temperature distribution, and differentiation. Am J Sci 267:1067–1082

Bottinga Y, Weill DF (1970) Density of liquid silicate systems calculated from partial molar volumes of oxide components. Am J Sci 269:169–182

Bowen NL, Andersen O (1914) The binary system $MgO-SiO_2$. Am J Sci 4th set, 37:487–500

Brandeis G, Jaupart C (1986) On the interaction between convection and crystallization in cooling magma chambers. Earth Planet Sci Lett 77:345–361

Campbell IH (1973) Aspects of the petrology of the Jimberlana Layered Intrusion of Western Australia. Unpublished PhD thesis, London University

Campbell IH (1978) Some problems with cumulus theory. Lithos 11:311–321

Campbell IH, Turner JS (1987) A laboratory investigation of assimilation at the top of a basaltic magma chamber. J Geol (in press)

Carslaw HS, Jaeger JC (1959) Conduction of heat in solids. Oxford University Press

Chen CF, Turner JS (1980) Crystallization in a double-diffusive system. J Geophys Res 85:2537–2593

Elthon D (1979) High magnesia liquids as the parental magma for ocean floor basalts. Nature 278:514–517

Hess GB (1972) Heat and mass transport during crystallization of the Stillwater igneous complex. Geol Soc Am Mem 132:503–520

Huppert HE, Sparks RSJ (1980) The fluid dynamics of a basaltic magma chamber replenished by influx of hot dense ultrabasic magma. Contrib Mineral Petrol 75:279–289

Huppert HE, Sparks RSJ (1984) Double-diffusive convection due to crystallization in magmas. Ann Rev Earth Planet Sci 12:11–37

Huppert HE, Sparks RSJ, Wilson JR, Hallworth MA (1986) Cooling and crystallization at an inclined plane. Earth Planet Sci Lett 79:319–328

Irvine TN (1970) Heat transfer during solidification of layered intrusions. I. Sheets and sills. Can J Earth Sci 7:1031–1061

Irvine TN, Keith DW, Todd SG (1983) The $J-M$ platinum-palladium reef of the Stillwater complex, Montana II: origin by double-diffusive convective magma mixing and implications for the Bushveld Complex. Econ Geol 78:1287–1334

Jackson ED (1961) Primary textures and mineral associations in the ultramafic zone of the Stillwater Complex, Montana. U.S.G.S. Prof. Paper 358

Jaupart C, Brandeis G (1986) The stagnant bottom layer of convecting magma chambers. Earth Planet Sci Lett 80:183–199

Jaupart C, Brandeis G, Allegre CJ (1984) Stagnant layers at the bottom of convecting magma chambers. Nature 308:535–358

McBirney AR, Noyes RM (1979) Crystallisation and layering of the Skaergaard Intrusion. J Petrol 20:487–554

Mo X, Carmichael ISE, Rivers M, Stebbins J (1982) Partial molar volume of FeO in multicomponent silicate liquids and the pressure dependence of oxygen fugacity in magmas. Mineral Mag 45:237–245

Morse SA (1986) Thermal structure of crystallizing magma with two-phase convection. Geol Mag 123:205–214

Nelson SA, Carmichael ISE (1979) Partial molar volumes of oxide components in silicate liquids. Contrib Mineral Petrol 71:117–124

Roeder PL (1975) Thermodynamics of element distribution in experimental mafic silicate-liquid systems. Fortschr Mineral 52:61–73

Roeder PL, Emslie RF (1970) Olivine-liquid equilibrium. Contrib Mineral Petrol 29:275–289

Shaw HR (1965) Comments on viscosity, crystal settling, and convection in granitic magmas. Am J Sci 263:120–152

Shaw HR (1972) Viscosities of magmatic silicate liquids: an empirical method of prediction. Am J Sci 272:870–893

Taylor HP Jr, Forester RW (1979) An oxygen isotope study of the Skaergaard Intrusion and its country rocks: a description of a 55 My.old fossil hydrothermal system. J Petrol 20:355–419

Turner JS (1973) Buoyancy effects in fluids. Cambridge University Press

Turner JS, Campbell IH (1986) Convection and mixing in magma chambers. Earth Sci Rev 23:255–352

Turner JS, Gustafson LB (1978) The flow of hot saline solutions from vents in the sea floor: some implications for exhalative sulfide and other ore deposits. Econ Geol 73:1082–1100

Wager LR, Deer WA (1939) Geological investigations in East Greenland, Pt III. The Petrology of the Skaergaard Inrusion, Kangerdlugssauq, East Greenland. Medd Grœnl 105:1–352

Wilson AH (1982) The geology of the Great "Dyke", Zimbabwe: the ultramafic rocks. J Petrol 23:240–292

Received December 8, 1986 / Accepted February 24, 1987